Environmental Science & Technology

pubs.acs.org/est

Article

Promotive Effects of Chloride and Sulfate on the Near-Complete Destruction of Perfluorocarboxylates (PFCAs) in Brine via Hydrogen-tuned 185-nm UV Photolysis: Mechanisms and Kinetics

Sitao Liu, Gongde Chen, Qingyang Shi, Jay Gan, Bosen Jin, Yujie Men, and Haizhou Liu*

Cite This: *Environ. Sci. Technol.* 2024, 58, 10347−10356

Read Online

ACCESS | Metrics & More | Article Recommendations | Supporting Information

ABSTRACT: Hydrogen-tuned 185 nm vacuum ultraviolet (VUV/H_2) photolysis is an emerging technology to destroy per- and polyfluoroalkyl substance (PFAS) in brine. This study discovered the promotive effects of two major brine anions, i.e., chloride and sulfate in VUV/H_2 photolysis on the hydrated electron (e^-_{aq}) generation and perfluorocarboxylates (PFCAs) destruction and established a kinetics model to elucidate the promotive effects on the steady-state concentration of e^-_{aq} ($[e^-_{aq}]_{ss}$). Results showed that VUV/H_2 achieved near-complete defluorination of perfluorooctanoic acid (PFOA) in the presence of up to 1000 mM chloride or sulfate at pH 12. The defluorination rate constant (k_{deF}) of PFOA peaked with a chloride concentration at 100 mM and with a sulfate concentration at 500 mM. The promotive effects of chloride and sulfate were attributed to an enhanced generation of e^-_{aq} via their direct VUV photolysis and conversion of additionally generated hydroxyl radical to e^-_{aq} by H_2, which was supported by a linear correlation between the predicted $[e^-_{aq}]_{ss}$ and experimentally observed k_{deF}. The k_{deF} value increased from pH 9 to 12, which was attributed to the speciation of the $H^{\cdot}/e^-_{aq}$ pair. Furthermore, the VUV system achieved >95% defluorination and ≥99% parent compound degradation of a concentrated PFCAs mixture in a synthetic brine, without generating any toxic perchlorate or chlorate.

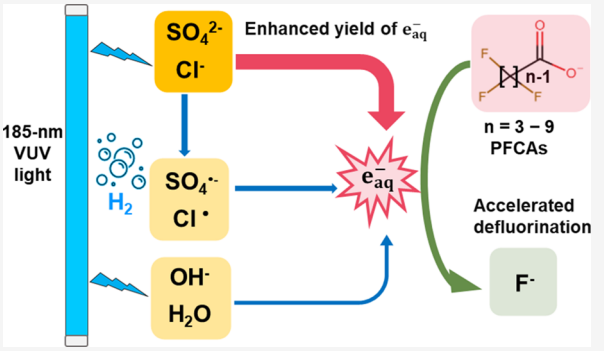

KEYWORDS: *PFAS, 185 nm UV, sulfate, chloride, hydrated electron, defluorination*

INTRODUCTION

Per- and polyfluoroalkyl substance (PFAS) pollution is an urgent global environmental issue. PFAS are ubiquitous,[1,2] recalcitrant to conventional treatment,[3,4] bioaccumulation,[5,6] and pose high public health risks.[7−9] Perfluorocarboxylates (PFCAs; $C_nF_{2n+1}COO^-$), one of the largest classes in the PFAS family, are persistent in the environment due to their strong C−F bonds,[10−13] resulting in the contamination of potable water.[14] The U.S. EPA recently updated the health advisory level for perfluorooctanoic acid (PFOA) at 0.004 ng/L[15] and proposed a maximum contaminant level (MCL) of 4 ng/L for PFOA in drinking water.[16] Perfluorononanoic acid (PFNA), another PFCA, has also been proposed with a hazard index MCL in drinking water by the U.S. EPA.[16] In addition, many states in the US have already established or are in the process of setting new regulatory standards for other PFCAs.[17]

Physical separation of PFAS, including ion exchange (IX)[18,19] and membrane filtration,[20−22] have been tested for drinking water treatment, through which PFAS are transferred into a brine waste stream. Consequently, PFAS treatment in brine waste has become a major challenge. For example, the regeneration of IX produces a brine with elevated PFAS and chloride.[19,23] The membrane concentrate is also elevated in salinity and PFAS levels.[24] Direct disposal of the brine poses a high risk of secondary contamination to drinking water. Therefore, there is an urgent need for the destruction of PFAS in brine. However, destroying PFAS in brine is challenging due to the complex water matrix. Existing technologies for aqueous PFAS destruction include electrochemical oxidation,[25,26] plasma treatment,[27] and UVC photolysis (λ = 254 nm),[28] but each has its limitations in brine treatment. Electrochemical PFAS oxidation in brine can produce toxic chlorate and perchlorate byproducts.[26,29] Plasma treatment is energy-intensive, with energy consumption ranging from 380 to 833 kWh/m^3 for PFOA treatment.[27] UVC photolysis requires the addition of photosensitizers (e.g., sulfite, iodide, and indole compounds) to produce hydrated electron (e^-_{aq}) that destroys PFAS,[28,30−32] but possesses relatively low quantum yields (Φ = 0.11−0.29) of e^-_{aq} from the photolysis of photosensitizer, and generates byproducts from photosensitizers.[32,33] Photocatalytic

Received: December 14, 2023
Revised: May 1, 2024
Accepted: May 3, 2024
Published: May 29, 2024

degradation of PFAS was achieved using boron nitride, with the formation of nitrate as a byproduct.[34]

In contrast, hydrogen-tuned vacuum UV (VUV/H_2) photolysis (λ = 185 nm) directly excites water molecules to selectively and efficiently form e_{aq}^- that destroys PFAS, without the need for any photosensitizer.[35] VUV/H_2 photolysis is fundamentally distinct from the conventional VUV process. Specifically, hydrogen gas (H_2) not only protects e_{aq}^- from quenching by dissolved oxygen but also transforms hydroxyl radical ($HO^{\cdot}$) into e_{aq}^-, which creates a e_{aq}^- dominant system. In contrast, conventional VUV photolysis has no selectivity to generate e_{aq}^- and generates nonselective hydroxyl radical ($HO^{\cdot}$) that aims for oxidative degradation of organic contaminants,[36−38] which has a limited capacity in PFCAs defluorination.[39] Furthermore, because water molecules strongly absorb 185 nm photons and have a high quantum yield to generate e_{aq}^- ($\Phi \approx 0.38$),[40,41] VUV/H_2 photolysis essentially turns abundant water molecules into e_{aq}^--based reducing agent, thus creating a sustainable, photosensitizers-free approach for PFAS destruction in contaminated source water.

Despite the promising advantages, little is known about the mechanisms and kinetics of VUV/H_2 photolysis for PFAS destruction in brine conditions, especially in the presence of chloride and sulfate as two major brine anions. First, although low mM levels of chloride and sulfate, typical in drinking water, were found to slightly promote the PFAS destruction during VUV/H_2 photolysis,[35] the effects of extremely high concentrations of chloride and sulfate in the regenerative IX brine and membrane concentrate, ranging from 10 mM to 1000 mM,[23,42,43] on the PFAS destruction kinetics and the mechanisms of e_{aq}^- generation remain unknown. Second, previous studies examined radical generation by chloride and sulfate under conventional oxidative VUV processes,[44−46] which were not relevant to the e_{aq}^--based reductive VUV/H_2 system. For example, the percentage of VUV light absorbed by each constituent will significantly change in response to different concentrations of chloride or sulfate, leading to unique radical pathways for e_{aq}^- reactions. Furthermore, there is a lack of quantitative understanding of the generation of e_{aq}^- under different levels of chloride and sulfate.

Third, the wide range of chloride and sulfate concentrations in brine results in varying ionic strengths, which can significantly impact the production of the e_{aq}^- and reaction kinetics, but the effects have not been quantified in the VUV/H_2 system. Additionally, the optimal pH of brine that favors PFAS destruction remains unknown. The commonly found pH in the brine concentrate is between 9 and 12,[26,47,48] which controls the acid−base speciation of hydrogen atom ($H^{\cdot}$) and e_{aq}^-, therefore significantly impacting the efficiency and kinetics of PFAS destruction.

Consequently, this study aimed to comprehensively examine the kinetics of PFCAs destruction and explore the mechanism of e_{aq}^- generation over a broad range of chloride and sulfate concentrations commonly found in regenerative IX brine and membrane concentrate. A theoretical reaction kinetic model was developed to quantify the steady-state concentration of e_{aq}^- in the VUV system. The effects of brine pH on the kinetics of PFOA defluorination were quantified. Following that, the kinetics of 7 PFCAs with various carbon chains (C3−C9) were evaluated in the VUV system under optimal chloride and sulfate concentrations. Finally, a synthetic brine containing a mixture of concentrated PFCAs was treated via 185 nm VUV/H_2 photolysis to demonstrate the near-complete destruction of PFCAs promoted by the presence of chloride and sulfate in brine.

MATERIALS AND METHODS

Chemicals. Analytical grade PFCAs ($C_nF_{2n+1}COO^-$; n = 3−9) were purchased from Sigma-Aldrich et al. An isotope-labeled PFAS internal standard mixture (MPFAC-24ES) was purchased from Wellington Laboratories. Detailed information on PFCAs used is provided in Table S1 in the Supporting Information (SI). All other solutions were prepared using >99% purity chemicals and with Milli-Q (resistivity > 18 MΩ·cm^{-1}) water unless otherwise noted. Selective experiments utilized a synthetic brine based on chloride and sulfate levels of a reverse osmosis (RO) concentrate from a brackish water desalination facility in inland Southern California[49] and spiked with elevated levels of PFCAs based on an IX regeneration brine (Table S2).[27]

Photochemical PFAS Destruction Experimental Setup. Photochemical reactions were conducted in a cylindrical borosilicate glass reactor wrapped with aluminum foil. The light source consisted of VUV lamps (LSE Inc.) enclosed in high-transmittance synthetic quartz sleeves (Suprasil 310, Heraeus) that were immersed in the solution. The 185 nm VUV fluence rate ($I_{a,185nm}$ = 6.5 × 10^{-6} Einstein·L^{-1}·s^{-1}) was measured using an established chemical actinometry method.[37] Details are provided in Text S1. The reactor was placed on a stir plate with a magnetic stir bar. A 500-mL solution containing 25 μM individual PFCA or a mixture of PFCA was prepared. The solution was presaturated with H_2 gas (99.999%) for 30 min and continuously purged throughout the reaction. The temperature was maintained at 25 °C by cooling the jacketed water. Droplets of 1 M NaOH were added to maintain the solution pH at the targeted level.

To evaluate the effects of chloride and sulfate on PFCA destruction, experiments with chloride or sulfate individually ranging from 0 to 1000 mM were conducted at a solution pH of 12. This pH was selected due to the fastest observed PFOA defluorination kinetics for both chloride and sulfate systems between pH 9 and 12. Next, the effects of solution pH ranging between 9 and 12 were investigated by using the optimal chloride and sulfate concentration identified above. To evaluate the significance of e_{aq}^- generation from the reaction between hydroxyl radical ($HO^{\cdot}$) and H_2, nitrogen (N_2) gas-saturated VUV control experiments (VUV/N_2) were conducted. In the N_2-saturated system, $HO^{\cdot}$ does not transform into e_{aq}^-. Therefore, the difference in PFOA destruction kinetics between N_2 and H_2 experiments represented the contribution of e_{aq}^- from $HO^{\cdot}$. To evaluate the roles of the oxidative radicals, e.g., reactive chlorine radicals and sulfate radical ($SO_4^{\cdot-}$) on PFOA destruction, nitrous oxide (N_2O) gas saturated VUV control experiments (VUV/N_2O) were performed to scavenge e_{aq}^- to exclusively leave oxidative radicals in the system. In addition, 254 nm UVC/H_2 control experiments were conducted with UVC lamps (LSE Inc.) in the same reactor configuration. To evaluate the treatment efficiency of PFCAs with different carbon chain lengths, 25 μM of individual PFCA ($C_nF_{2n+1}COO^-$; n = 3−9) was treated under optimal chloride, sulfate, and pH conditions identified above. Finally, a concentrated mixture of PFCAs in a synthetic brine was treated.

Chemical Analysis. The concentration of fluoride was measured by a fluoride ion selective electrode (Orion Star A214, Thermo Scientific). Before each use, the electrode was

https://doi.org/10.1021/acs.est.3c10552
Environ. Sci. Technol. 2024, 58, 10347−10356

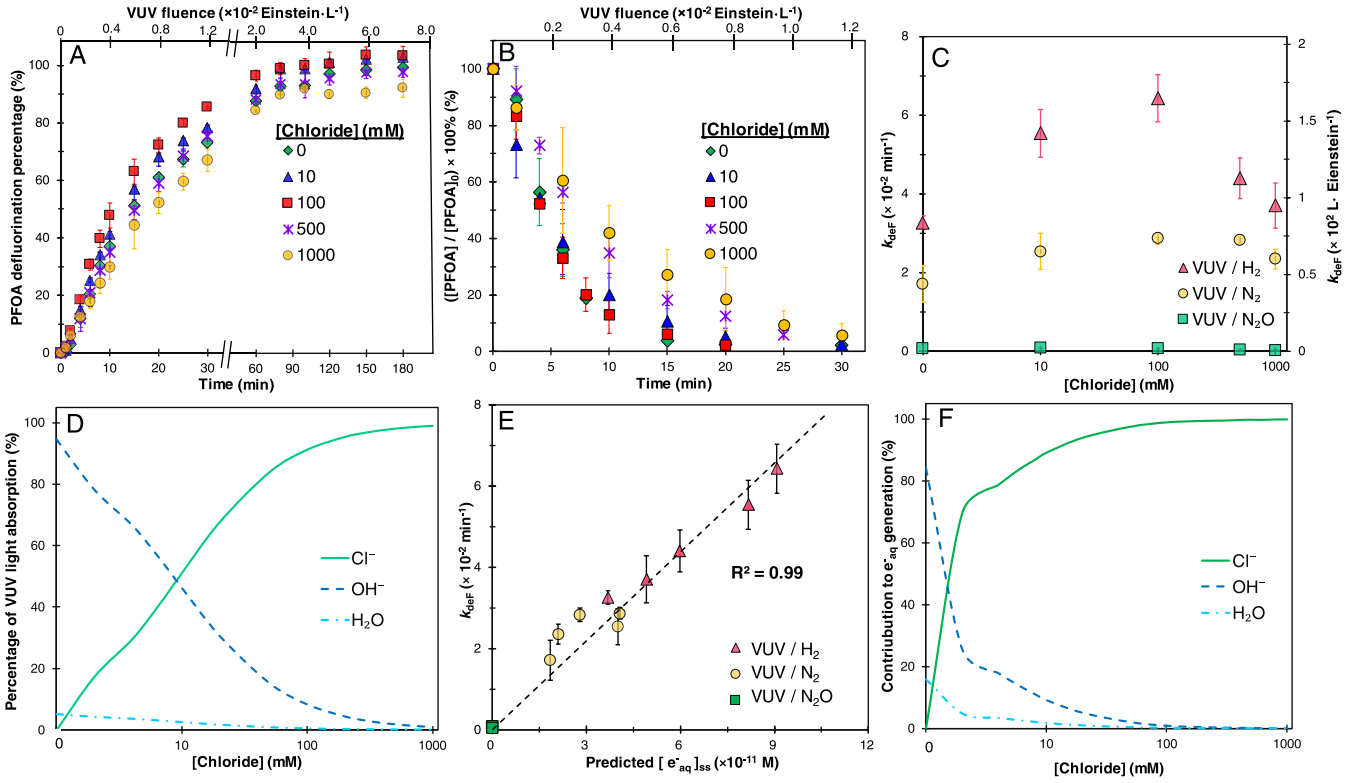

Figure 1. Effects of chloride on the destruction of PFOA and photochemistry of VUV/H_2 system. (A) Time profile of PFOA defluorination via VUV/H_2 photolysis; (B) time profile of PFOA degradation via VUV/H_2 photolysis; (C) *pseudo* first-order defluorination rate constant of PFOA in VUV photolysis under H_2 gas, N_2 gas, and N_2O gas tuned systems; (D) percentage of VUV light absorbed by each water constituent; (E) linear correlation between predicted $[e^-_{aq}]_{ss}$ and observed k_{deF} under VUV photolysis in the presence of chloride. (F) Model predicted contribution to e^-_{aq} generation from Cl^-, OH^-, and H_2O via VUV/H_2 photolysis. Initial [PFOA] = 25 μM; pH = 12. Error bars represent the differences between duplicate experiments and data points represent the average.

calibrated with standard NaF solutions in the presence of varying concentrations of chloride or sulfate. The method was validated and cross-checked by ion chromatography (IC) (DX-120, Thermo Fisher Scientific). The accuracy was also verified by a fluoride spike test, with a recovery rate of 100% ± 1%. The defluorination percentage was calculated as the molar percentage of fluoride ions measured at a given reaction time with respect to the total fluorine atoms in the PFCA initially present in the solution. Carbonate concentration was measured using the standard titration method.[50] The concentrations of chlorite, chlorate, and perchlorate were also analyzed by IC. Concentrations of PFCAs were measured by an ultra-performance liquid chromatograph equipped with a high-resolution quadrupole orbitrap mass spectrometer (UPLC–HRMS/MS, Thermo Scientific) or Waters ACQUITY UPLC system coupled with a Waters Micromass triple quadrupole (TQD) mass spectrometer equipped with an electrospray ionization source (Waters, Milford, MA). Solid phase extraction (SPE) was conducted to remove residual salinity from the samples before PFAS analysis. More Details are provided in Text S2.

RESULTS AND DISCUSSION

Impacts of Chloride on PFOA Destruction Kinetics via VUV/H_2 Photolysis. The presence of chloride initiated the PFOA destruction, with 90% defluorination achieved after 80 min of reaction (Figure 1A) and more than 95% PFOA parent compound degradation after 30 min of reaction (Figure 1B). Defluorination and degradation of PFOA followed *pseudo* first-order kinetics (Figure S2). The defluorination rate constant (k_{deF}) and *pseudo* first-order PFOA parent compound degradation rate constant (k_{deg}) were quantified as the slopes of first-order kinetics for the first 20 min shown in Figure S2. The first 20 min was chosen to capture the *pseudo* first-order kinetics trend to the best accuracy. Kinetics data showed that 100 mM chloride promoted PFOA defluorination at pH 12, with the k_{deF} nearly doubled from $(3.26 \pm 0.12) \times 10^{-2}$ min^{-1} (or $(0.84 \pm 0.03) \times 10^2$ L·Einstein^{-1}) to $(6.43 \pm 0.43) \times 10^{-2}$ min^{-1} (or $(1.65 \pm 0.11) \times 10^2$ L·Einstein^{-1}) as the chloride concentration increased from 0 to 100 mM (Figure 1C). In contrast, when the chloride concentration further increased from 100 to 1000 mM, the k_{deF} decreased by 42% to $(3.70 \pm 0.41) \times 10^{-2}$ min^{-1} (or $(0.95 \pm 0.10) \times 10^2$ L·Einstein^{-1}) compared to 100 mM, similar to the rate without chloride (Figure 1C). The k_{deg} followed a similar trend, with the maximal rate observed at 100 mM chloride (Figure S3). In addition, chlorite, chlorate, and perchlorate were not detected throughout the VUV/H_2 photolysis.

Chloride initiates a cascade of chain reactions in the VUV/H_2 system. First, chloride undergoes direct photolysis at 185 nm irradiation to generate e^-_{aq} and $Cl^{\cdot}$ (R1 in Scheme 1; all subsequent reactions refer to Scheme 1 and Table S3).[51] Meanwhile, water and hydroxide (OH^-) are photolyzed by 185 nm photons into a combination of $H^{\cdot}$, e^-_{aq} and $HO^{\cdot}$ (R2–4).[41,51,52] Second, $Cl^{\cdot}$ further reacts with OH^- and chloride to form $HOCl^{\cdot-}$ via two radical pathways (R5 vs R6–7, branching ratio calculated in Text S3).[53−55] Once $HOCl^{\cdot-}$ is produced, it rapidly dissociates into $HO^{\cdot}$ and Cl^- (R8).[56] The additional

https://doi.org/10.1021/acs.est.3c10552
Environ. Sci. Technol. 2024, 58, 10347−10356

Scheme 1. Reaction Scheme for H_2-Saturated VUV System in the Presence of Chloride and Sulfate[a]

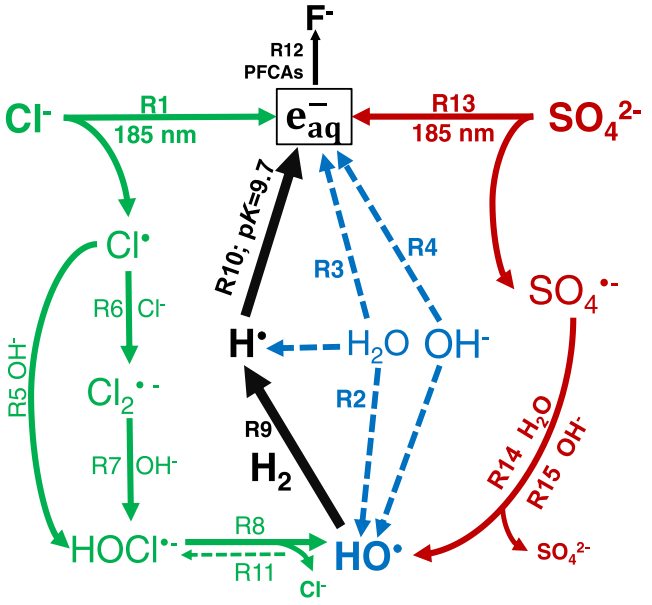

[a]Green line represents the reactions responsible for generating e^-_{aq} via chloride photolysis. Red line represents the reactions responsible for generating e^-_{aq} via sulfate photolysis. Blue-dashed line represents the reactions responsible for generating e^-_{aq} from water and OH^- photolysis. Black line represents the generation of e^-_{aq} from $HO^{\cdot}$.

$HO^{\cdot}$ originated from $Cl^{\cdot}$ is converted to $H^{\cdot}$ by dissolved H_2 (R9). e^-_{aq} is the predominant species in the $H^{\cdot}/e^-_{aq}$ acid–base couple when solution pH is higher than its pK values (R10; pK = 9.7).[57] Therefore, e^-_{aq} is produced via $Cl^{\cdot}$ chain reactions in VUV/H_2 systems in the presence of chloride (R5–10). Third, a chloride level higher than desirable can scavenge $HO^{\cdot}$ and reverse it to $HOCl^{\cdot-}$ (R11),[56] thus inhibiting the e^-_{aq} yield.

Additional VUV/N_2O and VUV/N_2 control experiments confirmed that e^-_{aq} was the major reactive species in the VUV/H_2 system, contributing to reductive PFOA defluorination. In the VUV/N_2O system, e^-_{aq} was quickly quenched by N_2O to form the $HO^{\cdot}/O^{\cdot-}$ pair (R16; p$K_{HO^{\cdot}/O^{\cdot-}}$ = 11.9; Text S3).[58] As a result, k_{deF} and k_{deg} were negligible in the VUV/N_2O system regardless of chloride levels (Figure 1C), which was consistent with prior observations that the oxidative radicals, such as $HO^{\cdot}$, $Cl^{\cdot}$, $Cl_2^{\cdot-}$ and $HOCl^{\cdot-}$, were not very effective in PFOA defluorination.[59−61] In the VUV/N_2 system, the absence of H_2 prevented $HO^{\cdot}$ to convert into e^-_{aq} (R9–10). The k_{deF} decreased by more than 50% in the VUV/N_2 compared to the VUV/H_2 system at each chloride level (Figure 1C), suggesting that the e^-_{aq} originated from direct photolysis of chloride, and OH^- and water contributed more than 50% to PFOA defluorination. Defluorination of PFOA by 254 nm UVC control was also negligible (Figure S4), suggesting that the 254 nm photons cannot initiate e^-_{aq} generation via the direct photolysis of chloride for PFAS destruction.

The presence of chloride at brine level significantly affected the production and reactivity of e^-_{aq} in 185 nm VUV/H_2 photolysis with three effects. First, chloride influences the percentage of VUV light absorption and further increases the production rate of e^-_{aq}. Chloride is a strong competitor for VUV light when added, with an absorption coefficient that is 5 orders of magnitude higher than water or comparable to OH^- ($\varepsilon_{Cl^-,185\ nm}$ = 3500 M^{-1} cm^{-1}; $\varepsilon_{OH^-,185\ nm}$ = 3200 M^{-1} cm^{-1}; ε_{H_2O} = 0.032 M^{-1} cm^{-1}).[40] Based on the percentage of VUV light absorption calculation (details provided in Text S4), VUV photons absorbed by chloride increased from 0 to 99% as chloride concentration increased from 0 to 1000 mM (Figure 1D), resulting in the shift of major e^-_{aq} initiator from OH^- to Cl^- (R1 vs R4). Moreover, the quantum yield of e^-_{aq} of chloride is much higher than OH^- ($\Phi_{Cl^-,185\ nm}$ = 0.43 vs $\Phi_{OH^-,185\ nm}$ = 0.11). To quantify the effects of chloride on the production of e^-_{aq}, the production rate of e^-_{aq} ($r_{e^-_{aq}}$) was calculated assuming $HO^{\cdot}$ and $Cl^{\cdot}$ are stoichiometrically transformed into e^-_{aq} in the VUV/H_2 system (detailed calculated shown in Text S4). Calculation showed that the presence of 1000 mM chloride increased the $r_{e^-_{aq}}$ by nearly 3.5 times compared to without chloride.

Second, when the chloride concentration was above 100 mM, it significantly quenched $HO^{\cdot}$ (R11) and consequently decreased the production of e^-_{aq} from $HO^{\cdot}$. When chloride was below 100 mM, R11 was more than 1 order of magnitude lower than R8, which led to a negligible scavenging effect of chloride on $HO^{\cdot}$ (Text S3). In this case, $HO^{\cdot}$ primarily reacted with H_2 to generate e^-_{aq}. At a chloride concentration higher than 100 mM, R11 began to scavenge $HO^{\cdot}$ significantly and R8 was suppressed.[62] For example, at 1000 mM, R11 is only 1.4 times lower than R8, which means that only 58% $HO^{\cdot}$ is available for transformation into e^-_{aq} (Text S3).

Third, the presence of chloride increased the ionic strength, which consequently increased the second-order rate constant between e^-_{aq} and PFOA (denoted as $k_{PFOA,e^-_{aq}}$) and decreased the quantum yield (detailed effects of ionic strength are summarized in Table S4). On the positive side, a higher ionic strength from a higher chloride concentration increases the $k_{PFOA,e^-_{aq}}$, due to increased shielding of like-charged reactants reducing the distance over which Coulombic forces repel the e^-_{aq} and PFOA.[63] A calculation based on Brønsted–Brjeuum equation showed that $k_{PFOA,e^-_{aq}}$ increased by a factor of 3.2 from 1.68×10^{-9} to 4.48×10^{-9} M^{-1} s^{-1} as chloride increased from 0 to 1000 mM (Figure S5A). On the negative side, the quantum yield of e^-_{aq} decreases by ∼10% as chloride concentration increases from 0 to 1000 mM (Figure S5B), based on a prior observation that the e^-_{aq} quantum yields via ClO_4^-, OH^-, and I^- 185-nm photolysis decreased by an average of 10% for every 1 M increased in ionic strength.[64] A high ionic strength decreases the survival probability of e^-_{aq}, which is related to the ion pairing effect with cations, e.g. Na^+.[64] When the chloride concentration exceeded 100 mM, the negative effects of chloride outweighed the positive effects, resulting in the lower k_{deF} and k_{deg}.

To further quantify the effects of chloride on e^-_{aq} generation via VUV/H_2 photolysis, the steady-state concentration of e^-_{aq}, $HO^{\cdot}$ and reactive chlorine species were calculated at different chloride concentrations considering the three effects from above (detailed calculations are provided in Text S5). In particular, the steady-state concentration of e^-_{aq} was calculated as following:

$$[e^-_{aq}]_{ss} = \frac{(I_{a,185nm}(\sum_{i=1}^{i} f_i \Phi_i) + k_{HO,H_2}[H_2][HO]_{ss})\alpha_{e^-_{aq}}}{\sum_{j=1}^{j} k_{e^-_{aq},j}[j]} \quad (1)$$

where $I_{a,185\ nm}$ is the volume-normalized 185-nm VUV fluence rate in this study (6.5×10^{-6} Einstein· L^{-1}·s^{-1}); f is the

https://doi.org/10.1021/acs.est.3c10552
Environ. Sci. Technol. 2024, 58, 10347−10356

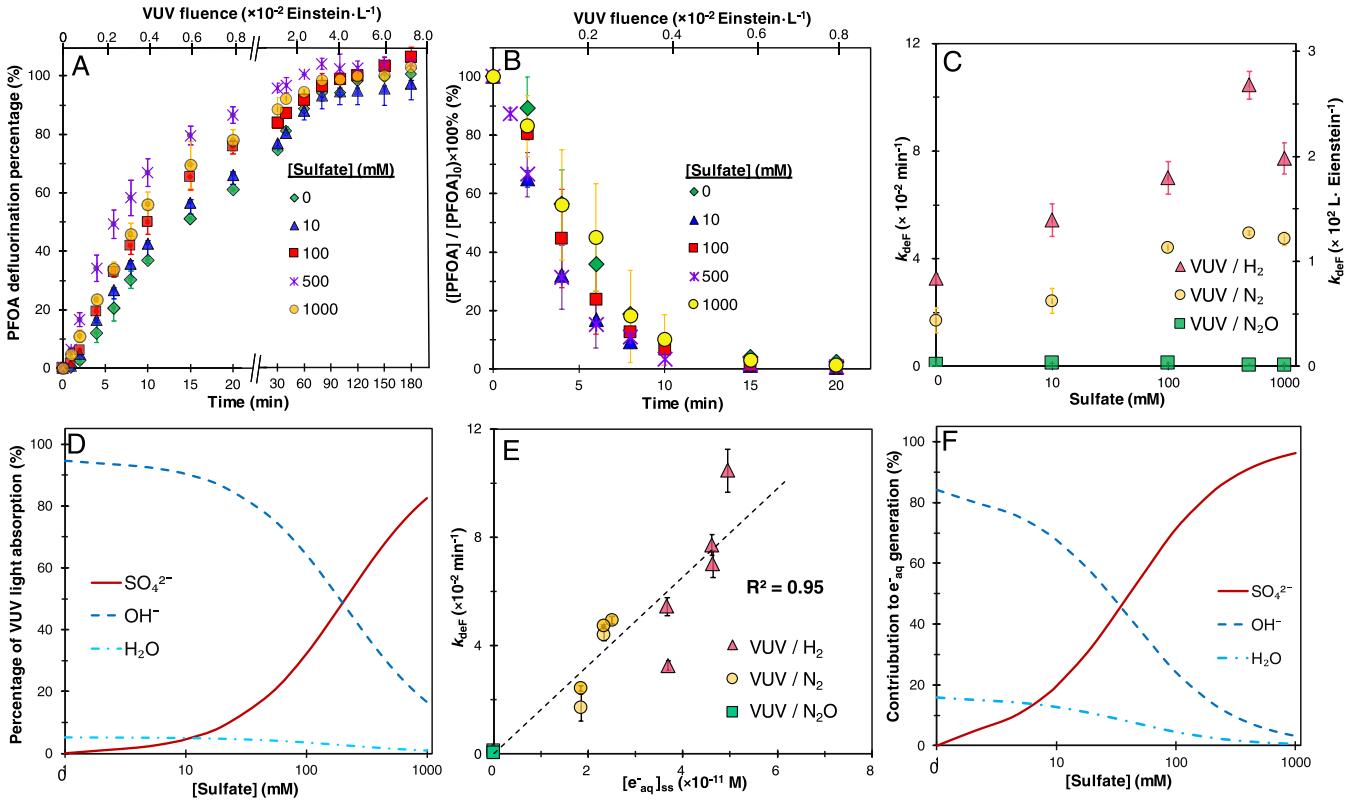

Figure 2. Effects of sulfate on the destruction of PFOA and photochemistry of VUV/H_2 system. (A) Time profile of PFOA defluorination via VUV/H_2 photolysis; (B) time profile of PFOA degradation via VUV/H_2 photolysis; (C) *pseudo* first-order defluorination rate constant of PFOA in VUV photolysis under H_2 gas, N_2 gas, and N_2O gas tuned systems; (D) percentage of VUV light absorbed by each water constituent; (E) linear correlation between predicted $[e^-_{aq}]_{ss}$ and observed k_{deF} in VUV photolysis in the presence of sulfate. (F) Model predicted contribution to e^-_{aq} generation from SO_4^{2-}, OH^-, and H_2O via VUV/H_2 photolysis. Initial [PFOA] = 25 μM; pH = 12. Error bars represent the differences between duplicate experiments, and data points represent the average.

percentage of VUV light absorbed by each chemical constituent (values shown in Figure 1D); Φ is the quantum yield of e^-_{aq} from each constituent (mol/Einstein; values shown in Table S3); $k_{HO^\cdot,H_2}$ is the second-order rate constant between H_2 and $HO^\cdot$ (6×10^7 M^{-1} s^{-1}); $[H_2]$ is the dissolved H_2 concentration (0.8 mM in this study); $[HO^\cdot]_{ss}$ is the steady-state concentration of $HO^\cdot$ (M; data shown in Table S5); $\alpha_{e^-_{aq}}$ is the speciation coefficient of e^-_{aq} depending on pH; $k_{e^-_{aq},j}$ is the second-order rate constant between e^-_{aq} and chemical constituents, including PFCAs and other potential scavengers (M^{-1} s^{-1}); $[j]$ are the concentrations of the chemical constituents (M).

The model predicted that the $[e^-_{aq}]_{ss}$ peaked at 100 mM of chloride in the VUV/H_2 system (Table S5). When combining the model predicted $[e^-_{aq}]_{ss}$ in VUV/N_2 and VUV/N_2O controls, the $[e^-_{aq}]_{ss}$ and the experimentally observed k_{deF} exhibited an extremely strong linear correlation, with a R^2 of 0.99 (Figure 1E). The $[e^-_{aq}]_{ss}$ also showed a good linear correlation with k_{deg}, with a R^2 of 0.92 (Figure S6A), confirming that chloride promoted e^-_{aq} concentration and accelerated PFOA destruction (R12). The model calculation showed that chloride contributed to more than 85% of e^-_{aq} generation with a concentration >10 mM (Figure 1F), mainly via chloride direct photolysis and the conversion of reactive chlorine species to e^-_{aq}. It is important to note that the predicted $[e^-_{aq}]_{ss}$ was only based on initial PFOA destruction during the first step of the defluorination process. As PFOA destruction continued, a mixture of transient short-chain PFAS intermediates was generated and subsequently destroyed. This destruction pathway was also observed during VUV photolysis in fresh water.[35] Moreover, the model only considered the major reaction pathways. Other pathways that consume e^-_{aq} such as the reaction between e^-_{aq} and $HO^\cdot$ or water are not considered. Therefore, the predicted $[e^-_{aq}]_{ss}$ highlighted the trend responding to different chloride concentrations, but may not exactly match the absolute values of $[e^-_{aq}]_{ss}$.

Impacts of Sulfate on PFOA Destruction Kinetics via VUV/H_2 Photolysis. The presence of sulfate strongly promoted extensive defluorination and rapid degradation of PFOA. Approximately 90% of defluorination was achieved in 60 min (Figure 2A) and 99% of PFOA degradation was achieved in 20 min in the presence of sulfate (Figure 2B). PFOA defluorination and degradation also followed a *pseudo* first-order kinetics in the presence of sulfate (Figure S7). PFOA destruction kinetics reached its maximum with 500 mM of sulfate. In particular, k_{deF} increased 3-fold from $(3.26 \pm 0.12) \times 10^{-2}$ min^{-1}, i.e., equivalent of $(0.84 \pm 0.03) \times 10^2$ L·Einstein^{-1}, to $(10.42 \pm 0.58) \times 10^{-2}$ min^{-1}, i.e., equivalent of $(2.68 \pm 0.15) \times 10^2$ L·Einstein^{-1} as sulfate increased from 0 to 500 mM and decreased slightly to $(7.72 \pm 0.28) \times 10^{-2}$ min^{-1} (equivalent of $(1.98 \pm 0.07) \times 10^2$ L·Einstein^{-1}) as sulfate further increased to 1000 mM (Figure 2C). The k_{deg} exhibited a maximum value (0.3 min^{-1}) at 500 mM sulfate as well (Figure S8).

Upon 185 nm VUV irradiation, sulfate is directly photolyzed into $SO_4^{\cdot-}$ and e^-_{aq} (R13).[51] At alkaline condition, $SO_4^{\cdot-}$ is

https://doi.org/10.1021/acs.est.3c10552
Environ. Sci. Technol. 2024, 58, 10347−10356

transformed into $HO^{\cdot}$ (R14 and R15) and subsequently e^-_{aq} (R9−10).[65] Both k_{deF} and k_{deg} in VUV/N_2O were negligible, confirming that e^-_{aq} was the major species for PFOA defluorination in the sulfate system (Figures 2C and S8). The defluorination rate in VUV/N_2 decreased by more than 50% compared to VUV/H_2, which indicated that the e^-_{aq} generated from direct photolysis of sulfate, OH^-, and water contributed to more than 50% of the PFOA defluorination.

The presence of sulfate affected the production and reactivity of e^-_{aq} in the VUV/H_2 systems in three ways. First, sulfate changed the percentage of VUV light absorption and the production of e^-_{aq} via direct 185 nm photolysis (ε = 260 M^{-1} cm^{-1}). As the sulfate concentration increased from 10 to 1000 mM, the VUV photons absorbed by sulfate increased from 4 to 83% (Text S4, Figure 2D). The quantum yield of e^-_{aq} via sulfate photolysis is approximately 6 times higher than that of OH^- ($\Phi_{SO_4^{2-}}$ = 0.67 mol/Einstein vs Φ_{OH^-} = 0.11 mol/Einstein), which leads to a 4.5 times higher $r_{e^-_{aq}}$ at 1000 mM sulfate compared to without sulfate (Text S4). Notably, the increase in $r_{e^-_{aq}}$ is 4.5-fold instead of 6-fold. This is because OH^- absorbs 17% of VUV photons in the presence of 1000 mM sulfate (Figure 2D), but its quantum yield is 6 times lower than that of sulfate. Second, sulfate enhanced the yield of $HO^{\cdot}$ and therefore generated e^-_{aq} via the reaction between $HO^{\cdot}$ and H_2. (R14-R15 followed by R9-R10). Unlike the reversible radical pathways of chloride, there were no scavenging reactions of $SO_4^{\cdot-}$ and $HO^{\cdot}$ to generate secondary radicals, Therefore, the production of e^-_{aq} from $HO^{\cdot}$ is positively related to sulfate concentration. Based on the calculation of $r_{e^-_{aq}}$, 50% of $r_{e^-_{aq}}$ was contributed from $SO_4^{\cdot-}$ if we assume that the $HO^{\cdot}$ generated from $SO_4^{\cdot-}$ was 100% transformed into e^-_{aq} (Text S4).

Third, sulfate changed the ionic strength, posing both positive and negative effects on the e^-_{aq} reactivity with PFAS and production. The increase in ionic strength results in a 4.4-fold increase in $k_{PFOA,e^-_{aq}}$ at 1000 mM sulfate compared to without sulfate (1.68×10^{-9} M^{-1} s^{-1} vs 6.16×10^{-9} M^{-1} s^{-1}; Figure S9A). In contrast, the ionic strength is ∼3 M at 1000 mM sulfate, which decreases the quantum yield of sulfate VUV photolysis (R13) by 30% (Figure S9B). Therefore, the combined effects resulted in an optimal sulfate level at 500 mM (Figures 2C and S8).

The predicted $[e^-_{aq}]_{ss}$ via VUV photolysis in the presence of sulfate peaked at 500 mM (Text S6, Table S6). The predicted $[e^-_{aq}]_{ss}$ and the experimentally observed k_{deF} and k_{deg} also exhibited a strong linear correlation, with R^2 values of 0.95 and 0.97 (Figures 2E and S6B), which strongly supported the mechanism of the sulfate system described above. The model calculation showed that sulfate absorbed a majority of the VUV photons when its concentration exceeded 200 mM (Figure 2D). Sulfate outcompeted OH^- and H_2O and became the dominant species in producing e^-_{aq}, which contributed more than 95% of e^-_{aq} generation as its concentration reached 1000 mM (Figure 2F).

Impact of pH on PFOA Destruction in the VUV/H_2 System with Chloride and Sulfate. Effects of the pH were evaluated at the optimal levels of chloride (100 mM) and sulfate (500 mM). The k_{deF} of PFOA destruction in the VUV/H_2 system increased from pH 9 to 12 in the presence of either chloride or sulfate (Figure 3A). The values of k_{deg} followed a similar trend, where the values between pH 11 and 12 were approximately 1.5 times higher than those between pH 9 and 10.5 (Figure S10). At the optimal pH and chloride or sulfate concentration, ≥99% of PFOA degradation was achieved within 20 min (Figure S11), and 100% was achieved after 3 h (Figure S12).

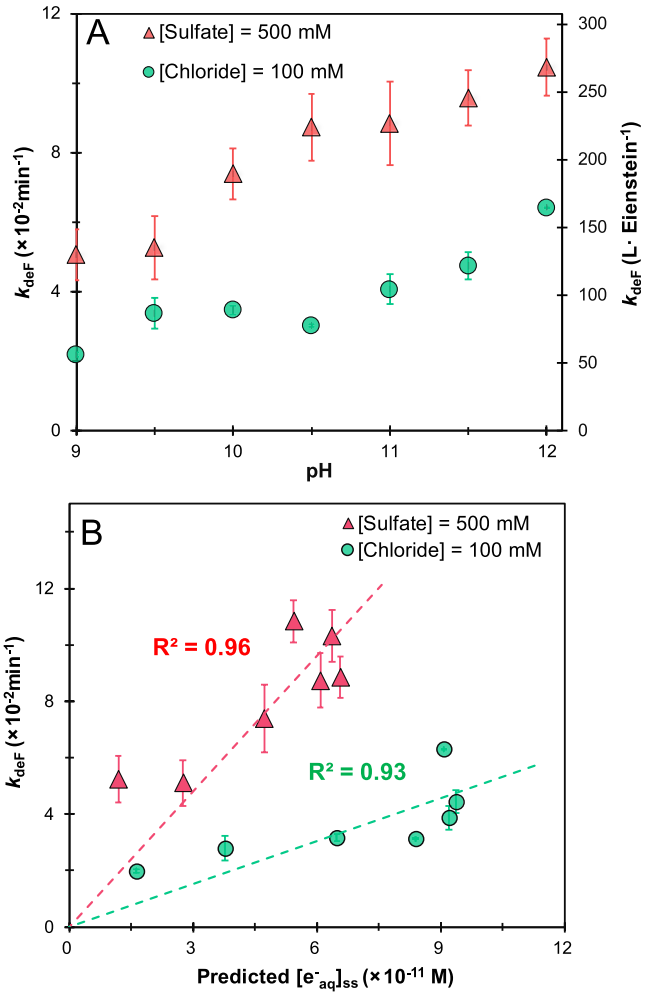

Figure 3. Effects of pH on *pseudo* first-order PFOA kinetic rate constant via 185 nm VUV/H_2 photolysis. (A) PFOA defluorination rate constant; (B) linear correlation between predicted $[e^-_{aq}]_{ss}$ and measured k_{deF} in different pHs. Initial [PFOA] = 25 μM. Error bars represent the differences between duplicate experiments, and data points represent the average.

There are two competing effects of pH on e^-_{aq} production. First, with a pK of $H^{\cdot}/e^-_{aq}$ pair 9.7, e^-_{aq} is the dominant species above pH 9.7. Accordingly, the percentage of e^-_{aq} in the $H^{\cdot}/e^-_{aq}$ pair increased from 16 to 99% as pH increased from 9 to 12 (eq S14), which resulted in an accelerated defluorination when the pH was above 10 (Figure 3A). Second, the pH alters the percentage of VUV light absorption and impacts the production rate of e^-_{aq}. Calculation showed that 97% of 185 nm photons were absorbed by sulfate at pH 9. As the solution pH increased from 9 to 12, OH^- competed with sulfate for photons (ε_{OH^-} = 3200 M^{-1} cm^{-1} vs $\varepsilon_{SO_4^{2-}}$ = 260 M^{-1} cm^{-1}), and photons absorption by sulfate decreased from 98 to 70% (Figure S13A). Because the quantum yield of OH^- is lower than that of SO_4^{2-} (0.11 vs 0.67), an increase in pH lowered the production rate of e^-_{aq}, which resulted in a decrease of k_{deg} at pH 12 in the sulfate system (Figure S10). In contrast, the percentage of VUV light absorption in the chloride system was

https://doi.org/10.1021/acs.est.3c10552
Environ. Sci. Technol. 2024, 58, 10347−10356

similar at pHs between 9 and 12 (Figure S13B). Chloride absorbed an overwhelming majority (>91%) of the 185 nm photons at all pHs, which resulted in a relatively stable k_{deg} in the chloride system within a pH range of 9−12 (Figure S9).

The predicted $[e^-_{aq}]_{ss}$ via VUV/H_2 photolysis at different pHs in the presence of either chloride or sulfate system were all well linearly correlated with the experimentally observed k_{deF}, with $R^2 > 0.9$ (Figure 3B). It is notable that the slope of the linear correlation was higher in the presence of sulfate than in the presence of chloride. This is because the ionic strength in the sulfate system was higher than the chloride system, which increased the $k_{PFOA,e^-_{aq}}$ and subsequently suppressed the $[e^-_{aq}]_{ss}$ while achieving a higher defluorination rate.

Defluorination Kinetics of PFCAs under Optimal Chloride and Sulfate Conditions. In the presence of 100 mM chloride, 90−100% defluorination of C3−C7 ($C_nF_{2n+1}COOH$, n = 3−7) PFCAs, 75% of C8 PFCA, and 66% of C9 PFCA were achieved (Figure 4A). In comparison, the presence of 500 mM sulfate effectively achieved 100% or nearly 100% defluorination of C3−7 PFCAs, and 80−90% C8−9 PFCAs after 3 h VUV/H_2 photolysis (Figure 4B). The presence of sulfate resulted in 2−3 times k_{deF} of PFCAs than chloride (Figure S14), which was similar to our previous results (Figures 1A and 2A). It is worth noting that the presence of sulfate rather than chloride can achieve a higher defluorination percentage of certain PFCAs, e.g., PFDA. It is because the sulfate system has a stronger promotive effect than the chloride system; 500 mM sulfate exhibited a 2-fold higher k_{deF} than 100 mM chloride. The sulfate system generates more e^-_{aq} than the chloride system, which can destroy PFAS byproduct more effectively and leads to a higher defluorination rate. In addition, the 80−90% defluorination upper limit for C8−C9 PFCAs may be attributed to the production of less-reactive intermediate products that need further study to understand the degradation pathways.

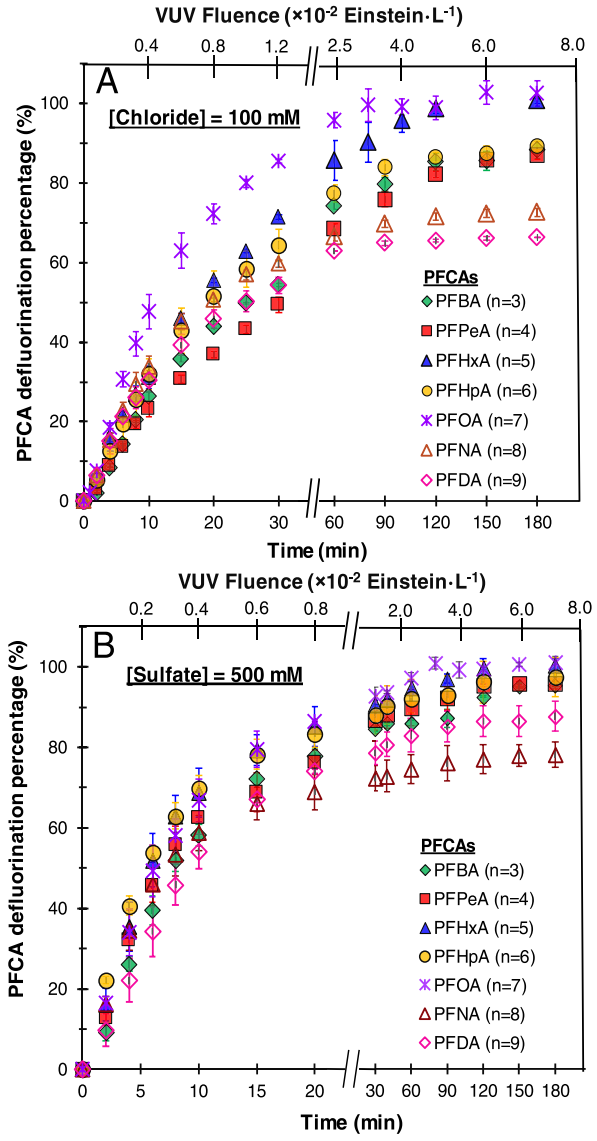

Figure 4. Defluorination of 7 PFCAs via VUV/H_2 photolysis. (A) Defluorination kinetics of individual PFCA; $[Cl^-]$ = 100 mM, [PFCA] = 25 μM; (B) defluorination kinetics of individual PFCA; $[SO_4^{2-}]$ = 500 mM, [PFCA] = 25 μM.

To further evaluate the new treatment platform, a concentrated mixture of PFCAs in a synthetic RO concentrate was treated by VUV/H_2 photolysis. In a 5-h treatment, >95% defluorination and nearly 100% degradation of the mixture of PFCAs were achieved (Figure S15 and Table S7). Therefore, our findings indicate that two major brine anions, chloride and sulfate, effectively improve the efficiency of VUV/H_2 for the destruction of PFCA in the brine concentrates.

Implications to PFAS Destruction Research and Engineering. Unique promotive effects of common anions in brine waste, specifically 100 mM chloride and 500 mM sulfate, were shown to accelerate PFAS destruction by increasing the production of e^-_{aq} associated with 185 nm VUV water photolysis. Considering the commonly found concentrations of chloride and sulfate in brine are 10−1000 mM, the VUV/H_2 system stands out as a potential technology to achieve complete PFAS destruction without introducing other photosensitizer chemical additives to the brine, therefore leaving no byproducts that require additional cleanup. Hydrogen gas (H_2) has been commonly used in biological nitrate and perchlorate reduction processes,[66,67] and its usage in industrial applications is safe following proper protocols. The electrical energy per order for destruction of PFOA (EE/O_{deg}) and electrical energy as 90% of the maximum defluorination percentage achieved (EE/O_{deF}) under various conditions in this lab study were calculated (Text S7 and Table S8). At optimal pH ranges (11.5−12), the EE/O_{deg} for the VUV/H_2 system in the brine waste was 7.7−17 kWh/m^3, and the EE/O_{deF} was 47−75 kWh/m^3. Although comparable electrical energy consumptions for PFOA removal were reported in other UV-based platforms, including VUV/boron nitride (EE/O_{deg} = 6.4 kWh/m^3) and UVC/sulfite iodide systems (EE/O_{deg} = 1.4 kWh/m^3 and EE/O_{deF} = 60 kWh/m^3),[28,34] the effects of salinity in the feedwater matrix on other UV-based platforms are unknown and a direct comparison is not applicable. Furthermore, energy consumption can be further optimized by a careful choice of high-efficiency UV lamps and high-transmittance quartz sleeves that produce the best photon energy efficiency.

To treat real brine waste, e^-_{aq} and $HO^{\cdot}$ scavengers in brine need to be carefully considered. Approximately 5 mM methanol may also coexist with chloride in IX brine after the distillation.[26] Although methanol reacts $HO^{\cdot}$ ($k_{HO^{\cdot},MeOH}$ = 8.3 × 10^8 M^{-1} s^{-1}), chloride has a higher reaction rate with $HO^{\cdot}$, and the concentration of chloride is much higher than methanol (R11 in Table S3). Therefore, the presence of

https://doi.org/10.1021/acs.est.3c10552
Environ. Sci. Technol. 2024, 58, 10347−10356

methanol has a limited effect. Carbonate poses both positive and negative effects on the VUV/H_2 process.[68] For the positive side, carbonate undergoes direct 185 nm VUV photolysis and generates e^-_{aq}.[46] For the negative effects, although carbonate has a low reactivity with e^-_{aq} ($k_{e^-_{aq},CO_3^{2-}}$ = 3.9 × 10^5 M^{-1} s^{-1}), it can react with $HO^{\cdot}$ rapidly ($k_{HO^{\cdot},CO_3^{2-}}$ = 4.0 × 10^8 M^{-1} s^{-1}) and inhibits the generation of e^-_{aq} from $HO^{\cdot}$. Dissolved organic matter (DOM) can quench e^-_{aq} ($k_{e^-_{aq},DOM}$ = 0.5−2.1 × 10^8 M^{-1} s^{-1})[69,70] and compete for VUV photons with chloride and sulfate. We previously reported that 5.4 mg-C/L humic acids had a negligible effect on the defluorination of PFOA.[35] However, the composition and concentration of DOM are heterogeneous and require a site-specific evaluation. DOM can also be removed by a pretreatment step. Nitrate ($k_{e^-_{aq},NO_3^-}$ = 9.2 × 10^9 M^{-1} s^{-1}) and nitrite ($k_{e^-_{aq},NO_2^-}$ = 3.5 × 10^9)[63,70] are also strong competitors with PFAS for e^-_{aq} and their presences need to be considered when designing VUV systems for PFAS destruction. For example, using the additional 254 nm photons in the same VUV lamps to photolyze photosensitizers for nitrate removal.[71−73]

■ ASSOCIATED CONTENT

Supporting Information

The Supporting Information is available free of charge at https://pubs.acs.org/doi/10.1021/acs.est.3c10552.

Detailed information for chemicals, detailed experiment procedure, sample analysis, and theoretical calculation procedures; figures for *pseudo-first-order* degradation kinetics for PFOA under different experimental conditions, degradation, and defluorination of PFOA at different pHs; tables for major reactions and energy consumption calculations (PDF)

■ AUTHOR INFORMATION

Corresponding Author

Haizhou Liu − *Department of Chemical and Environmental Engineering, University of California, Riverside, California 92521, United States;* orcid.org/0000-0003-4194-2566; Phone: (951) 827-2076; Email: haizhou@engr.ucr.edu; Fax: (951) 827-5696

Authors

Sitao Liu − *Department of Chemical and Environmental Engineering, University of California, Riverside, California 92521, United States;* orcid.org/0000-0003-1043-9220

Gongde Chen − *Department of Chemical and Environmental Engineering, University of California, Riverside, California 92521, United States*

Qingyang Shi − *Department of Environmental Sciences, University of California, Riverside, California 92521, United States*

Jay Gan − *Department of Environmental Sciences, University of California, Riverside, California 92521, United States;* orcid.org/0000-0002-7137-4988

Bosen Jin − *Department of Chemical and Environmental Engineering, University of California, Riverside, California 92521, United States;* orcid.org/0000-0001-7659-3437

Yujie Men − *Department of Chemical and Environmental Engineering, University of California, Riverside, California 92521, United States;* orcid.org/0000-0001-9811-3828

Complete contact information is available at: https://pubs.acs.org/10.1021/acs.est.3c10552

Notes

The authors declare no competing financial interest.

■ ACKNOWLEDGMENTS

This research was supported by the U.S. National Science Foundation PFAS-ERASE Initiatives (CBET-2131745) and I-Corps Program (TIP-2310201), and UC Riverside Proof-of-Concept Grant. We thank Nimai Plouffe, Andrew Abdala and Genivee Gast at UCR for assisting with photochemical experiments and Mingrui Song for analyzing synthetic brine samples. We also thank Ken Ishida, Meeta Pannu, and Megan Plumlee at Orange County Water District for their feedback on the manuscript.

■ REFERENCES

(1) Hu, X. C.; Andrews, D. Q.; Lindstrom, A. B.; Bruton, T. A.; Schaider, L. A.; Grandjean, P.; Lohmann, R.; Carignan, C. C.; Blum, A.; Balan, S. A.; Higgins, C. P.; Sunderland, E. M. Detection of Poly- and Perfluoroalkyl Substances (PFASs) in U.S. Drinking Water Linked to Industrial Sites, Military Fire Training Areas, and Wastewater Treatment Plants. *Environ. Sci. Technol. Lett.* **2016**, *3* (10), 344−350.

(2) Glüge, J.; Scheringer, M.; Cousins, I. T.; Dewitt, J. C.; Goldenman, G.; Herzke, D.; Lohmann, R.; Ng, C. A.; Trier, X.; Wang, Z. An Overview of the Uses of Per- and Polyfluoroalkyl Substances (PFAS). *Environ. Sci.: Process Impacts* **2020**, *22* (12), 2345−2373.

(3) Schultz, M. M.; Higgins, C. P.; Huset, C. A.; Luthy, R. G.; Barofsky, D. F.; Field, J. A. Fluorochemical Mass Flows in a Municipal Wastewater Treatment Facility. *Environ. Sci. Technol.* **2006**, *40* (23), 7350−7357.

(4) Loganathan, B. G.; Sajwan, K. S.; Sinclair, E.; Senthil Kumar, K.; Kannan, K. Perfluoroalkyl Sulfonates and Perfluorocarboxylates in Two Wastewater Treatment Facilities in Kentucky and Georgia. *Water. Res.* **2007**, *41* (20), 4611−4620.

(5) Haukås, M.; Berger, U.; Hop, H.; Gulliksen, B.; Gabrielsen, G. W. Bioaccumulation of Per- and Polyfluorinated Alkyl Substances (PFAS) in Selected Species from the Barents Sea Food Web. *Environ. Pollut.* **2007**, *148* (1), 360−371.

(6) Liu, Z.; Lu, Y.; Song, X.; Jones, K.; Sweetman, A. J.; Johnson, A. C.; Zhang, M.; Lu, X.; Su, C. Multiple Crop Bioaccumulation and Human Exposure of Perfluoroalkyl Substances around a Mega Fluorochemical Industrial Park, China: Implication for Planting Optimization and Food Safety. *Environ. Int.* **2019**, *127*, 671−684.

(7) Nguyen, G. T. H.; Nocentini, A.; Angeli, A.; Gratteri, P.; Supuran, C. T.; Donald, W. A. Perfluoroalkyl Substances of Significant Environmental Concern Can Strongly Inhibit Human Carbonic Anhydrase Isozymes. *Anal. Chem.* **2020**, *92* (6), 4614−4622.

(8) Nian, M.; Luo, K.; Luo, F.; Aimuzi, R.; Huo, X.; Chen, Q.; Tian, Y.; Zhang, J. Association between Prenatal Exposure to PFAS and Fetal Sex Hormones: Are the Short-Chain PFAS Safer? *Environ. Sci. Technol.* **2020**, *54* (13), 8291−8299.

(9) Zheng, G.; Schreder, E.; Dempsey, J. C.; Uding, N.; Chu, V.; Andres, G.; Sathyanarayana, S.; Salamova, A. Per- And Polyfluoroalkyl Substances (PFAS) in Breast Milk- And Trends for Current-Use PFAS. *Environ. Sci. Technol.* **2021**, *55* (11), 7510−7520.

(10) Salavati-Fard, T.; Wang, B. Significant Role of Oxygen Dopants in Photocatalytic PFCA Degradation over H-BN. *ACS Appl. Mater. Interfaces.* **2021**, *13* (39), 46727−46737.

(11) Park, H.; Vecitis, C. D.; Cheng, J.; Choi, W.; Mader, B. T.; Hoffmann, M. R. Reductive Defluorination of Aqueous Perfluorinated Alkyl Surfactants: Effects of Ionic Headgroup and Chain Length. *J. Phys. Chem. A* **2009**, *113* (4), 690−696.

(12) Conder, J. M.; Hoke, R. A.; De Wolf, W.; Russell, M. H.; Buck, R. C. Are PFCAs Bioaccumulative? A Critical Review and

Comparison with Regulatory Criteria and Persistent Lipophilic Compounds. *Environ. Sci. Technol.* **2008**, *42* (4), 995−1003.
(13) Trang, B.; Li, Y.; Xue, X. S.; Ateia, M.; Houk, K. N.; Dichtel, W. R. Low-Temperature Mineralization of Perfluorocarboxylic Acids. *Science (1979)* **2022**, *377* (6608), 839−845.
(14) Ng, C.; Cousins, I. T.; DeWitt, J. C.; Glüge, J.; Goldenman, G.; Herzke, D.; Lohmann, R.; Miller, M.; Patton, S.; Scheringer, M.; Trier, X.; Wang, Z. Addressing Urgent Questions for PFAS in the 21st Century. *Environ. Sci. Technol.* **2021**, *55* (19), 12755−12765.
(15) *Drinking Water Health Advisories for PFOA and PFOS | US EPA*. https://www.epa.gov/sdwa/drinking-water-health-advisories-pfoa-and-pfos (accessed Nov 4, 2023).
(16) *Per- and Polyfluoroalkyl Substances (PFAS) | US EPA*. https://www.epa.gov/sdwa/and-polyfluoroalkyl-substances-pfas (accessed Nov 4, 2023).
(17) *Safer States: PFAS*. https://www.saferstates.com/toxic-chemicals/pfas/ (accessed Jan 29, 2023).
(18) Liu, Y. L.; Sun, M. Ion Exchange Removal and Resin Regeneration to Treat Per- and Polyfluoroalkyl Ether Acids and Other Emerging PFAS in Drinking Water. *Water Res.* **2021**, *207*, No. 117781.
(19) Boyer, T. H.; Fang, Y.; Ellis, A.; Dietz, R.; Choi, Y. J.; Schaefer, C. E.; Higgins, C. P.; Strathmann, T. J. Anion Exchange Resin Removal of Per- and Polyfluoroalkyl Substances (PFAS) from Impacted Water: A Critical Review. *Water Res.* **2021**, *200*, No. 117244.
(20) Steinle-Darling, E.; Reinhard, M. Nanofiltration for Trace Organic Contaminant Removal: Structure, Solution, and Membrane Fouling Effects on the Rejection of Perfluorochemicals. *Environ. Sci. Technol.* **2008**, *42* (14), 5292−5297.
(21) Mastropietro, T. F.; Bruno, R.; Pardo, E.; Armentano, D. Reverse Osmosis and Nanofiltration Membranes for Highly Efficient PFASs Removal: Overview. *Challenges and Future Perspectives. Dalton Trans.* **2021**, *50* (16), 5398−5410.
(22) Xiong, J.; Hou, Y.; Wang, J.; Liu, Z.; Qu, Y.; Li, Z.; Wang, X. The Rejection of Perfluoroalkyl Substances by Nanofiltration and Reverse Osmosis: Influencing Factors and Combination Processes. *Environ. Sci.: Water Res. Technol.* **2021**, *7* (11), 1928−1943.
(23) Liu, Z.; Haddad, M.; Sauvé, S.; Barbeau, B. Alleviating the Burden of Ion Exchange Brine in Water Treatment: From Operational Strategies to Brine Management. *Water Res.* **2021**, *205*, No. 117728.
(24) Mccleaf, P.; Stefansson, W.; Ahrens, L. Drinking Water Nanofiltration with Concentrate Foam Fractionation-A Novel Approach for Removal of per-and Polyfluoroalkyl Substances (PFAS). *Water Res.* **2023**, *232*, No. 119688.
(25) Maldonado, V. Y.; Becker, M. F.; Nickelsen, M. G.; Witt, S. E. Laboratory and Semi-Pilot Scale Study on the Electrochemical Treatment of Perfluoroalkyl Acids from Ion Exchange Still Bottoms. *Water (Basel)* **2021**, *13* (20), 2873.
(26) Wang, L.; Nickelsen, M.; Chiang, S. Y.; Woodard, S.; Wang, Y.; Liang, S.; Mora, R.; Fontanez, R.; Anderson, H.; Huang, Q. Treatment of Perfluoroalkyl Acids in Concentrated Wastes from Regeneration of Spent Ion Exchange Resin by Electrochemical Oxidation Using Magnéli Phase Ti4O7 Anode. *Chem. Eng. J. Adv.* **2021**, *5*, No. 100078.
(27) Singh, R. K.; Multari, N.; Nau-Hix, C.; Woodard, S.; Nickelsen, M.; Mededovic Thagard, S.; Holsen, T. M. Removal of Poly- And Per-Fluorinated Compounds from Ion Exchange Regenerant Still Bottom Samples in a Plasma Reactor. *Environ. Sci. Technol.* **2020**, *54* (21), 13973−13980.
(28) Liu, Z.; Chen, Z.; Gao, J.; Yu, Y.; Men, Y.; Gu, C.; Liu, J. Accelerated Degradation of Perfluorosulfonates and Perfluorocarboxylates by UV/Sulfite + Iodide: Reaction Mechanisms and System Efficiencies. *Environ. Sci. Technol.* **2022**, *56* (6), 3699−3709.
(29) Wang, Y.; Li, L.; Huang, Q. Electrooxidation of Per- and Polyfluoroalkyl Substances in Chloride-Containing Water on Surface-Fluorinated Ti4O7 Anodes: Mitigation and Elimination of Chlorate and Perchlorate Formation. *Chemosphere* **2022**, *307*, No. 135877.
(30) Kugler, A.; Dong, H.; Li, C.; Gu, C.; Schaefer, C. E.; Choi, Y. J.; Tran, D.; Spraul, M.; Higgins, C. P. Reductive Defluorination of Perfluorooctanesulfonic Acid (PFOS) by Hydrated Electrons Generated upon UV Irradiation of 3-Indole-Acetic-Acid in 12-Aminolauric-Modified Montmorillonite. *Water Res.* **2021**, *200*, No. 117221.
(31) Chen, Z.; Teng, Y.; Mi, N.; Jin, X.; Yang, D.; Wang, C.; Wu, B.; Ren, H.; Zeng, G.; Gu, C. Highly Efficient Hydrated Electron Utilization and Reductive Destruction of Perfluoroalkyl Substances Induced by Intermolecular Interaction. *Environ. Sci. Technol.* **2021**, *55* (6), 3996−4006.
(32) Bentel, M. J.; Yu, Y.; Xu, L.; Li, Z.; Wong, B. M.; Men, Y.; Liu, J. Defluorination of Per- and Polyfluoroalkyl Substances (PFASs) with Hydrated Electrons: Structural Dependence and Implications to PFAS Remediation and Management. *Environ. Sci. Technol.* **2019**, *53* (7), 3718−3728.
(33) Yu, K.; Li, X.; Chen, L.; Fang, J.; Chen, H.; Li, Q.; Chi, N.; Ma, J. Mechanism and Efficiency of Contaminant Reduction by Hydrated Electron in the Sulfite/Iodide/UV Process. *Water Res.* **2018**, *129*, 357−364.
(34) Qanbarzadeh, M.; DiGiacomo, L.; Bouteh, E.; Alhamdan, E. Z.; Mason, M. M.; Wang, B.; Wong, M. S.; Cates, E. L. An Ultraviolet/Boron Nitride Photocatalytic Process Efficiently Degrades Poly-/Perfluoroalkyl Substances in Complex Water Matrices. *Environ. Sci. Technol. Lett.* **2023**, *10* (8), 705−710.
(35) Chen, G.; Liu, S.; Shi, Q.; Gan, J.; Jin, B.; Men, Y.; Liu, H. Hydrogen-Polarized Vacuum Ultraviolet Photolysis System for Enhanced Destruction of Perfluoroalkyl Substances. *J. Hazard. Mater. Lett.* **2022**, *3*, No. 100072.
(36) Li, M.; Qiang, Z.; Hou, P.; Bolton, J. R.; Qu, J.; Li, P.; Wang, C. VUV/UV/Chlorine as an Enhanced Advanced Oxidation Process for Organic Pollutant Removal from Water: Assessment with a Novel Mini-Fluidic VUV/UV Photoreaction System (MVPS). *Environ. Sci. Technol.* **2016**, *50* (11), 5849−5856.
(37) Masjoudi, M.; Mohseni, M. Photochemical Properties of Free Chlorine and Inorganic Chloramines at 185 Nm for VUV/UV/Chlorine Advanced Oxidation. *ACS ES&T Water* **2022**, *2* (5), 769−777.
(38) Li, M.; Li, W.; Bolton, J. R.; Blatchley, E., III; Qiang, Z. Organic Pollutant Degradation in Water by the Vacuum-Ultraviolet/Ultraviolet/H2O2 Process: Inhibition and Enhancement Roles of H2O2. *Environ. Sci. Technol.* **2018**, *53* (2), 912−918.
(39) Esfahani, E. B.; Zeidabadi, F. A.; Mohseni, M. Vacuum-UV Radiation Capable of Catalyst-Free Decomposition of 6:2 FTSA: The Transformation Mechanism and Impacts of the Water Matrix. *ACS ES&T Water* **2023**, *3* (11), 3614−3625.
(40) Weeks, J. L.; Meaburn, G. M.; Gordon, S. Absorption Coefficients of Liquid Water and Aqueous Solutions in the Far Ultraviolet. *Radiat. Res.* **1963**, *19*, 559−567.
(41) Gonzalez, M. G.; Oliveros, E.; Wörner, M.; Braun, A. M. Vacuum-Ultraviolet Photolysis of Aqueous Reaction Systems. *J. Photo. Photo. C: Photo Rev.* **2004**, *5* (3), 225−246.
(42) Arias-Paić, M. S.; Korak, J. A. Forward Osmosis for Ion Exchange Waste Brine Management. *Environ. Sci. Technol. Lett.* **2020**, *7* (2), 111−117.
(43) Van Der Bruggen, B.; Lejon, L.; Vandecasteele, C. Reuse, Treatment, and Discharge of the Concentrate of Pressure-Driven Membrane Processes. *Environ. Sci. Technol.* **2003**, *37* (17), 3733−3738.
(44) Duca, C.; Imoberdorf, G.; Mohseni, M. Effects of Inorganics on the Degradation of Micropollutants with Vacuum UV (VUV) Advanced Oxidation. *J. Environ. Sci. Health A* **2017**, *52* (6), 524−532.
(45) Furatian, L.; Mohseni, M. Influence of Chloride on the 185 nm Advanced Oxidation Process. *Chemosphere* **2018**, *199*, 263−268.
(46) Furatian, L.; Mohseni, M. Influence of Major Anions on the 185 nm Advanced Oxidation Process - Sulphate, Bicarbonate, and Chloride. *Chemosphere* **2018**, *201*, 503−510.
(47) Gao, Y.; Deng, S.; Du, Z.; Liu, K.; Yu, G. Adsorptive Removal of Emerging Polyfluoroalky Substances F-53B and PFOS by Anion-

Exchange Resin: A Comparative Study. *J. Hazard. Mater.* **2017**, *323*, 550−557.
(48) Deng, S.; Yu, Q.; Huang, J.; Yu, G. Removal of Perfluorooctane Sulfonate from Wastewater by Anion Exchange Resins: Effects of Resin Properties and Solution Chemistry. *Water Res.* **2010**, *44* (18), 5188−5195.
(49) Tang, X.; Kum, S.; Liu, H. Inland Desalination Brine Disposal: A Baseline Study from Southern California on Brine Transport Infrastructure and Treatment Potential. *ACS EST Eng.* **2022**, *2* (3), 456−464.
(50) Rice, E.; Baird, R.; Eaton, A.; Cleceri, L. *Standard Methods for the Examination of Water and Wastewater Method 2320*, 22nd ed.; American Public Health Association: Washington, DC, 2012.
(51) Dainton, F. S.; Fowles, P. The Photolysis of Aqueous Systems at 1849 Å II. Solutions Containing Cl-, Br-, SO2−4 or OH- Ions. *Proc. R Soc. Lond A Math Phys. Sci.* **1965**, *287* (1410), 312−327.
(52) Zoschke, K.; Börnick, H.; Worch, E. Vacuum-UV Radiation at 185nm in Water Treatment - A Review. *Water Res.* **2014**, *52*, 131−145.
(53) Klaning, U. K.; Wolff, T. Laser Flash Photolysis of HCIO, CIO−, HBrO, and BrO−in Aqueous Solution. Reactions of Cl- and Br-Atoms. *Berichte der Bunsengesellschaft für physikalische Chemie* **1985**, *89* (3), 243−245.
(54) Nagarajan, V.; Fessenden, R. W. Flash Photolysis of Transient Radicals. 1. X2- with X = Cl, Br, I, and SCN. *J. Phys. Chem.* **1985**, *89*, 2330−2335.
(55) Grigor'ev, A. E.; Makarov, I. E.; Pikaev, A. K. Formation of Cl2- in the Bulk of Solution during Radiolysis of Concentrated Aqueous Solutions of Chlorides. *Khimiya Vysokikh Ehnergij* **1987**, *21* (2), 123−126.
(56) Jayson, G. G.; Parsons, B. J.; Swallow, A. J. Some Simple, Highly Reactive, Inorganic Chlorine Derivatives in Aqueous Solution. Their Formation Using Pulses of Radiation and Their Role in the Mechanism of the Fricke Dosimeter. *Journal of the Chemical Society, Faraday Transactions 1: Physical Chemistry in Condensed Phases* **1973**, *69* (0), 1597−1607.
(57) Walker, D. C. The Hydrated Electron. *Quarterly Reviews, Chemical Society* **1967**, *21* (1), 79−108.
(58) Buxton, G. V.; Greenstock, C. L.; Helman, W. P.; Ross, A. B. Critical Review of Rate Constants for Reactions of Hydrated Electrons, Hydrogen Atoms and Hydroxyl Radicals (·OH/·O−) in Aqueous Solution. *J. Phys. Chem. Ref. Data* **2009**, *17* (2), 513.
(59) Hori, H.; Hayakawa, E.; Einaga, H.; Kutsuna, S.; Koike, K.; Ibusuki, T.; Kiatagawa, H.; Arakawa, R. Decomposition of Environmentally Persistent Perfluorooctanoic Acid in Water by Photochemical Approaches. *Environ. Sci. Technol.* **2004**, *38* (22), 6118−6124.
(60) Javed, H.; Lyu, C.; Sun, R.; Zhang, D.; Alvarez, P. J. J. Discerning the Inefficacy of Hydroxyl Radicals during Perfluorooctanoic Acid Degradation. *Chemosphere* **2020**, *247*, No. 125883.
(61) Metz, J.; Zuo, P.; Wang, B.; Wong, M. S.; Alvarez, P. J. J. Perfluorooctanoic Acid Degradation by UV/Chlorine. *Environ. Sci. Technol. Lett.* **2022**, *9* (8), 673−679.
(62) Buxton, G. V.; Bydder, M.; Salmon, G. A. Reactivity of Chlorine in Aqueous Solution Part 1 The Equilibrium ClMNsbd+Cl-Cl2. *J. Chem. Soc., Faraday Trans.* **1998**, *94* (5), 653−657.
(63) Fennell, B. D.; Mezyk, S. P.; McKay, G. Critical Review of UV-Advanced Reduction Processes for the Treatment of Chemical Contaminants in Water. *ACS Environ. Au* **2022**, *2*, 178−205.
(64) Sauer, M. C.; Shkrob, I. A.; Lian, R.; Crowell, R. A.; Bartels, D. M.; Chen, X.; Suffern, D.; Bradforth, S. E. Electron Photodetachment from Aqueous Anions. 2. Ionic Strength Effect on Geminate Recombination Dynamics and Quantum Yield for Hydrated Electron. *J. Phys. Chem. A* **2004**, *108* (47), 10414−10425.
(65) Redpath, J. L.; Willson, R. L. Chain Reactions and Radiosensitization: Model Enzyme Studies. *Int. J. Radiat. Biol.* **1975**, *27*, 389−398.
(66) Chung, J.; Nerenberg, R.; Rittmann, B. E. Evaluation for Biological Reduction of Nitrate and Perchlorate in Brine Water Using the Hydrogen-Based Membrane Biofilm Reactor. *J. Environ. Eng.* **2007**, *133* (2), 157−164.
(67) Zhao, H. P.; Van Ginkel, S.; Tang, Y.; Kang, D. W.; Rittmann, B.; Krajmalnik-Brown, R. Interactions between Perchlorate and Nitrate Reductions in the Biofilm of a Hydrogen-Based Membrane Biofilm Reactor. *Environ. Sci. Technol.* **2011**, *45* (23), 10155−10162.
(68) Nash, K.; Mulac, W.; Noon, M.; Fried, S.; Sullivan, J. C. Pulse Radiolysis Studies of U(VI) Complexes in Aqueous Media. *J. Inorg. Nucl. Chem.* **1981**, *43* (5), 897−899.
(69) Fennell, B. D.; Fowler, D.; Mezyk, S. P.; McKay, G. Reactivity of Dissolved Organic Matter with the Hydrated Electron: Implications for Treatment of Chemical Contaminants in Water with Advanced Reduction Processes. *Environ. Sci. Technol.* **2023**, *57* (19), 7634−7643.
(70) Fennell, B. D.; Odorisio, A.; Mckay, G. Quantifying Hydrated Electron Transformation Kinetics in UV-Advanced Reduction Processes Using the Re-. *UV Method. Environ. Sci. Technol.* **2022**, *56* (14), 10329−10338.
(71) Chen, G.; Hanukovich, S.; Chebeir, M.; Christopher, P.; Liu, H. Nitrate Removal via a Formate Radical-Induced Photochemical Process. *Environ. Sci. Technol.* **2019**, *53* (1), 316−324.
(72) Yuan, Y.; Feng, L.; He, X.; Wu, M.; Ai, Z.; Zhang, L.; Gong, J. Nitrate Promoted Defluorination of Perfluorooctanoic Acid in UV/Sulfite System: Coupling Hydrated Electron/Reactive Nitrogen Species-Mediated Reduction and Oxidation. *Environ. Pollut.* **2022**, *313*, No. 120172.
(73) Ren, Z.; Bergmann, U.; Leiviskä, T. Reductive Degradation of Perfluorooctanoic Acid in Complex Water Matrices by Using the UV/Sulfite Process. *Water Res.* **2021**, *205*, No. 117676.

https://doi.org/10.1021/acs.est.3c10552
Environ. Sci. Technol. 2024, 58, 10347−10356